# C-H and Si-H Activation Reactions at Ru/Ga Complexes: A Combined Experimental and Theoretical Case Study on the Ru-Ga Bond

Maximilian Muhr, Raphael Bühler, Hao Liang, Jonas Gilch, Christian Jandl, Samia Kahlal, Jean-Yves Saillard, Christian Gemel, Roland A Fischer

Chemistry–A European Journal
Research Article
doi.org/10.1002/chem.202200887
Chemistry Europe
European Chemical Societies Publishing
www.chemeurj.org

# C–H and Si–H Activation Reactions at Ru/Ga Complexes: A Combined Experimental and Theoretical Case Study on the Ru–Ga Bond

Maximilian Muhr[+],[a] Raphael Bühler[+],[a] Hao Liang,[b] Jonas Gilch,[a] Christian Jandl,[a] Samia Kahlal,[b] Jean-Yves Saillard,*[b] Christian Gemel,[a] and Roland A. Fischer*[a]

**Abstract:** Treatment of [Ru(COD)(MeAllyl)$_2$] and [Ru(COD)(COT)] with GaCp* under hydrogenolytic conditions leads to reactive intermediates which activate Si–H or C–H bonds, respectively. The product complexes [Ru(GaCp*)$_3$(SiEt$_3$)H$_3$] (**1**) and [Ru(GaCp*)$_3$(C$_7$H$_7$)H$_3$] (**2**) are formed with HSiEt$_3$ or with toluene as the solvent, respectively. While **1** was isolated and fully characterized by NMR, MS, IR and SC-XRD, **2** was too labile to be isolated and was observed and characterized in situ by using mass spectrometry, including labelling experiments for the unambiguous assignment of the elemental composition. The structural assignment was confirmed by DFT calculations. The relative energies of the four isomers possible upon toluene activation at the *ortho*-, *meta*-, *para*- and CH$_3$-positions have been determined and point to aromatic C–H activation. The Ru–Ga bond was analyzed by EDA and QTAIM and compared to the Ru–P bond in the analogue phosphine compound. Bonding analyses indicate that the Ru-GaCp* bond is weaker than the Ru-PR$_3$ bond.

## Introduction

Cooperative effects between transition metals TM and electropositive metals E (e.g. group 12 and 13 elements) play an important role in bond activation reactions of small molecules,[1–9] both in molecular compounds, as well as intermetallic solid-state materials.[10–12] The cooperative effects are mostly attributed to the electronic properties of intermetallic bonds, featuring electrophilic centers E($\delta^+$) in direct vicinity to an electron rich TM($\delta^-$) with pronounced reductive character.[13–16] Key examples are the Ni/Al complex [(Cp*Al)$_3$Ni(μ-H)Al(C$_6$H$_5$)($\eta^1$-Cp*], which is formed by C–H activation of C$_6$H$_6$ (benzene) at the coordinatively unsaturated 16 VE intermediate [Ni(AlCp*)$_3$],[17] and the Rh/Ga complex [Cp*Rh{$\eta^5$-C$_5$Me$_4$Ga(CH$_3$)$_3$}], which is formed by C–C activation of Cp*.[18] DFT calculations revealed that the electrophilic character of the gallium center favors the crucial C–C activation reaction step, allowing the reaction to proceed under extremely mild conditions.

Unsaturated Ruthenium phosphine complexes [Ru(PR$_3$)$_n$] (n = 3, 4) are well-established and are known to activate H–H,[19–21] C–H[22] and C–C[23] bonds. Berry and co-workers reported on an oxidative-addition/reductive-elimination equilibrium of different substituted silanes in [Ru(PMe$_3$)$_4$(SiR$_3$)H].[24] The same complex is also capable of activating the C–H bond of benzene in a sequence of similar reactions. They also report the formation of the polyhydride [Ru((PMe$_3$)$_3$(SiEt$_3$)H$_3$] from [Ru(PMe$_3$)$_4$H$_2$].[24]

[Ru(GaCp*)$_3$H$_2$], which is formed by H–H activation, has been identified as an intermediate in the formation of the cluster [(GaCp*)$_4$HRu(μ-Ga)RuH$_2$(GaCp*)$_3$].[25]

In the light of these results and the fact, that experimental as well as theoretical studies support the isolobal relation between GaCp* and phosphines[26–32] we were interested to investigate the reactivity of the unsaturated [Ru(GaCp*)$_3$H$_2$] in C–H and Si–H bond activation in the context of cluster growth.

The complex [(Ru(GaCp*)$_3$(SiEt$_3$)H$_3$] (**1**) is obtained from [Ru(COD)(MeAllyl)$_2$] (COD = 1,5-cyclooctadiene; MeAllyl = 2-methylallyl) and GaCp* in HSiEt$_3$ under hydrogenolytic conditions, whereas in less reactive solvents (*n*-hexane, cyclohexane), uncontrolled cluster growth is observed. Complex **1** is a structural analogue to [Ru(PMe$_3$)$_3$(SiEt$_3$)H$_3$]. It was characterized via SC-XRD, NMR, MS, IR, Raman, UV/Vis and elemental analysis. The analogous complex [Ru(GaCp*)$_3$(C$_7$H$_7$)H$_3$] (**2**) is formed upon C–H activation of toluene and was identified by high-resolution mass spectrometry, with DFT calculations allowing the assignment of a plausible structure. Finally, we performed a detailed comparison of the Ru–Ga and Ru–P

[a] M. Muhr,[+] R. Bühler,[+] J. Gilch, Dr. C. Jandl, Dr. C. Gemel, Prof. Dr. R. A. Fischer
Chair of Inorganic and Metalorganic Chemistry
Department of Chemistry
Catalysis Research Center (CRC)
Technical University Munich (TUM)
Lichtenbergstraße 4, 85748 Garching (Germany)
E-mail: roland.fischer@tum.de

[b] H. Liang, Dr. S. Kahlal, Prof. Dr. J.-Y. Saillard
UMR-CNRS, 6226 "Institut des Sciences Chimiques de Rennes"
Univ Rennes, CNRS, ISCR-UMR 6226
35000 Rennes (France)
E-mail: jean-yves.saillard@univ-rennes1.fr

[+] These authors contributed equally to this work.

Supporting information for this article is available on the WWW under https://doi.org/10.1002/chem.202200887

bondings, including energy decomposition analysis (EDA) and quantum theory of atoms in molecules (QTAIM) analysis.

## Results and Discussion

### Synthesis and characterization $[Ru(GaCp^*)_3(SiEt_3)H_3]$ (1)

The stoichiometric reaction (based on the Ru/Ga ratio) of $[Ru(COD)(MeAllyl)_2]$ (COD = 1,5-cyclooctadiene; MeAllyl = 2-methylallyl) with three equivalents of GaCp* in triethylsilane under 3 bar $H_2$ pressure leads to a dark orange solution after 6 h at 60 °C (Figure 1a). After removing all volatiles *in vacuo*, yellow crystals suitable for single crystal x-ray diffraction (SC-XRD) of **1** can be obtained by recrystallization from *n*-hexane at −30 °C. SC-XRD reveals a ruthenium centered complex, tetrahedrally surrounded by three GaCp* ligands and one $SiEt_3$ unit (Figure 1b). The compound's architecture is isostructural to Berry's complex $[Ru(PMe_3)_3(SiEt_3)H_3]$. It should be noted that the hydride ligands could not be located with final certainty in the structure refinement. The Ru–Ga bond lengths, which vary only slightly from 2.376(3) Å to 2.385(6) Å, as well as the Ga–$Cp^*_{centroid}$ distances (1.970–1.982 Å), are in good agreement with distances reported in the literature.[25,33–35] The Ru–Si bond length (2.373(2) Å) also matches Ru–Si bond lengths reported in the literature.[36,37] Notably, it only differs 0.003 Å from the isostructural $[Ru(PMe_3)_3(SiEt_3)H_3]$.[24] The tetrahedral structure is distorted, due to the three sterically demanding GaCp*, resulting in Ga–Ru-Si angles ranging from 118.1° to 121.0°.

The $^1$H NMR gives the expected set of signals for the three GaCp* ($\delta$ = 1.88 ppm, s, 45 H) and the three ethyl groups of the silyl ($\delta$ = 1.26 ppm, t, 9 H; $\delta$ = 0.92 ppm, q, 6 H). This is in good agreement with the $^{13}$C signals: The Cp* ligand (ring carbon at $\delta$ = 113.5 ppm and methyl groups at $\delta$ = 10.0 ppm), as well as the silyl-ethyl signals for $CH_3$ ($\delta$ = 10.5 ppm) and $CH_2$ groups ($\delta$ = 20.2 ppm). Moreover, the $^1$H NMR shows one broad singlet at $\delta$ = -13.31 ppm with a relative intensity equivalent to 2.7, strongly indicating the presence of three hydrides similar to $[Ru(PMe_3)_3(SiEt_3)H_3]$. The presence of hydrides is further supported by vibrational spectroscopy: In the infrared spectrum an intensive broad band at 1898 $cm^{-1}$, along with a small shoulder at 1771 $cm^{-1}$ is present in the typical Ru–H region. The expected band in the Raman spectrum, is observed at 1913 $cm^{-1}$ (Figure S24). High resolution liquid injection field desorption ionization mass spectrometry (LIFDI-MS) gives rise to a signal for $[M-2H]^{+\bullet}$ (m/z = 832.131; calc = 832.134), we attribute the loss of two H atoms to fragmentation. Based on the SC-XRD structural data of **1**, its geometry was fully optimized by DFT calculations at the BP86/TZ2P level (see Computational Details). In analogy to the molecular structure of $[Ru(PMe_3)_3(SiEt_3)H_3]$[24], the structure of lowest energy found for **1** (confirmed as a minimum by frequency calculations) corresponds to a configuration in which the three hydrides are located in an umbrella-like arrangement (Figure 1c). The DFT-simulated spectrum (Figure S22) is in reasonable agreement with the experimental data, showing Ru–H bands at 1985 $cm^{-1}$ (symmetric stretch), 1961 $cm^{-1}$ and 1942 $cm^{-1}$ (both asymmetric stretches). This optimized structure is in very good agreement with the crystal structure. Ru–Ga and Ru–Si bonds only differ by less than 0.005 Å, and bond angles of the 'metal core' (Ru/Ga/Si) only by less than 4°. The computed Si…H distances (2.067 Å–2.155 Å) are indicative of no bonding interaction. All calculated Ru–H distance are almost equivalent, ranging from 1.626 to 1.631 Å. The computed H–H distances (2.404 Å–2.493 Å) indicate classical hydride ligands rather than dihydrogen-bonding. This is confirmed in a $T_1$ relaxation NMR experiment (Figure S5), with $T_1$(min) = 546–1231 ms (193 K–293 K). The computed $^1$H hydride chemical shifts (−10.3 ppm) are 3 ppm lower than their experimental counterparts, whereas the other computed $^1$H signals differ by less than 1 ppm than their observed homologues. The same situation is found for the hydride signal in the related complex $[Ru(PMe_3)_3(SiEt_3)H_3]$ (computed: −7.7 ppm; recorded −10.53 ppm[24]), whereas the average deviation of all other proton signals is also less than 1 ppm. All these results strongly support the trihydride nature of **1**.

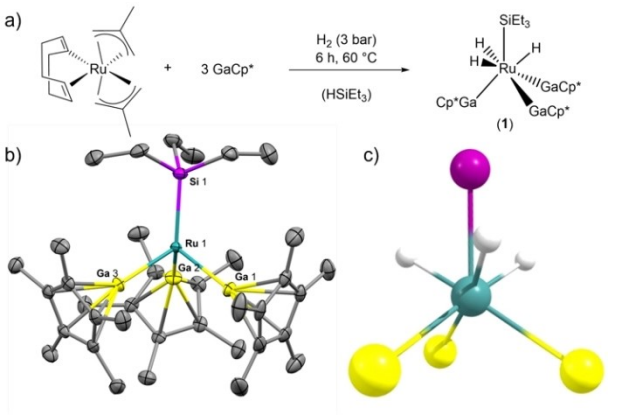


**Figure 1.** a) Reaction scheme for the synthesis of **1**. b) Molecular structure of $[Ru(GaCp^*)_3(SiEt_3)H_3]$ (**1**). Ellipsoids at the 50% probability level. H atoms are omitted for clarity. Selected bond lengths (Å) and angles (deg): Ru1–Ga1 = 2.376(3), Ru1–Ga2 = 2.376(4), Ru1–Ga3 = 2.385(6), Ru1–Si1 = 2.373(2), Ga–$Cp^*_{cent}$ = 1.970-1.982; Ga1–Ru1–Ga2 = 96.43(2), Ga1–Ru1–Ga3 = 99.36(2), Ga2–Ru1–Ga3 = 97.29(2), Ga1–Ru1–Si1 = 120.98(2), Ga2–Ru1–Si1 = 119.73(2), Ga3–Ru1–Si1 = 118.10(3). Space group: P 1 21/c 1. c) DFT-optimized structure (BP86/TZ2P) showing the hydrides' positions. Ru-H = 1.626–1.631 Å; Si-H = 2.067–2.155 Å Other C and H atoms omitted for clarity.

### C-H activation of toluene: $[Ru(GaCp^*)_3(C_7H_7)H_3]$ (2)

After observing that Si–H bonds can be activated, we wanted to investigate whether C–H bonds can also be activated in a similar manner. Thus $[Ru(COD)(MeAllyl)_2]$ and [Ru(COD)(COT)] (COT = 1,3,5-cyclooctatriene) were reacted with GaCp* under analogous reaction conditions to **1** in toluene. Both reactions lead to dark brown solutions even after a short time of 20 minutes. Notably, the formation of **1** seems to be slower as judged by the color change to orange after six hours. LIFDI-MS suggests the formation of a series of toluene containing compounds. As shown by experiments with different Ru precursors, the nature of the Ru source is important for the

product distribution, however, differences become prominent only after prolonged reaction times. After one hour the reaction solutions of [Ru(COD)(MeAllyl)$_2$]/GaCp* as well as [Ru(COD)(COT)]/GaCp* in toluene contain products producing the same series of ions, which can be assigned to different toluene containing species: $[Ru_2(GaCp^*)_4(C_7H_8)H_2]^{+\bullet}$ (*m/z* = 1116.056; *calc* = 1116.058), $[Ru_2(Ga)(GaCp^*)_3(C_7H_8)H]^{+\bullet}$ (*m/z* = 980.933; *calc* = 980.933), $[Ru_2(GaCp^*)_3(C_7H_8)H_2]^{+\bullet}$ (*m/z* = 912.015; *calc* = 912.014), $[Ru(GaCp^*)_3(C_7H_8)H_2]^{+\bullet}$ (*m/z* = 810.109; *calc* = 810.110), $[Ru(GaCp^*)_2(C_7H_8)]^{+\bullet}$ (*m/z* = 604.051; *calc* = 604.051). While the mass spectrum of the reaction solution of [Ru(COD)(COT)]/GaCp* remains largely unchanged over time, the mass spectrum of the reaction solution of [Ru(COD)(MeAllyl)$_2$]/GaCp* reveals almost exclusively the ion $[Ru(GaCp^*_3)(C_7H_7)H_3]^{+\bullet}$ (**2**$^{+\bullet}$) after 48 h. We conclude from the measured sum formula that this signal does not represent a fragment but rather the molecular ion **2**$^{+\bullet}$, since the corresponding neutral complex **2** satisfies the 18 valence electron (VE) rule and is isoelectronic to **1**. A pattern at *m/z* = 604.051 ($[Ru(GaCp^*)_2(C_7H_8)]^{+\bullet}$) is assigned to the fragment $[M\text{-}GaCp^*\text{-}2H]^{+\bullet}$ of **2** (Figure 2a). These assignments and the composition of **2** could be confirmed by double labelling experiments with toluene-d$_8$ (Figure 2b) and with the mono ethyl-substituted derivative GaCp*$^{Et}$ (Cp*$^{Et}$ = 1-ethyl-2,3,4,5-tetramethylcyclopentadienyl) (Figure 2c), revealing the expected *m/z* differences of respectively 8 and 42 (three additional $CH_2$ groups).

In contrast to **1**, compound **2** could not be isolated. It is formed in solution after long reaction times and can be enriched, although some thermal degradation in solution is also observed then, becoming obvious from the formation of metallic precipitate and mirror. We also noticed a stark influence of the concentration, i.e. **2** can be enriched only when working at low concentrations ($c_{total} < 5$ mg/mL). Combined with the unstable nature of **2** under reduced pressure, it was thus impossible to crystalize the compound or to characterize enriched/pure samples with solution spectroscopic techniques (NMR, IR). Nevertheless $^1$H NMR of reaction solutions shows hydride signals (−14.15, −15.63, −16.03 and −16.22 ppm, Figure S6), as does the IR spectrum with bands at 1807 and 1861 cm$^{-1}$ (Figure S23). Inspired by the thermal induced reductive elimination of $HSiEt_3$ from $[(Cp^*Al)_3NiH(SiEt_3)]$ yielding $[(Cp^*Al)_3Ni(\mu\text{-}H)Al(C_6H_5)(\eta^1\text{-}Cp^*]$ by subsequent C–H activation of benzene,[17] we attempted the preparation of a pure sample of **2** from thermal treatment of **1** in toluene. Even under harsh conditions, no reaction was observed. A similar behavior was observed for the treatment of a solution of **2** with an excess of $HSiEt_3$.

As no experimental access to structural data was possible, reasonable structures representing energy minima for the postulated trihydride complex **2** were calculated on the DFT level of theory. The energetically most favorable structures correspond to activated toluene in *ortho*, *meta*, *para* and benzylic position, respectively (Figure 3). Their computed relative energies indicate that the products upon C–H activation at an aromatic position are almost equal in energy and are favored with respect to the activation at the benzylic position. The energy difference between the *ortho* and *meta* isomers is insignificant and that of the *para* relative is barely larger. Thus, even if not considering the possibility of topological isomerism for each individual *ortho*, *meta* and *para* system, the possibility of having several isomers in solution should not be excluded. These calculations only reflect thermodynamic stability. In order to investigate differences in regioselectivity between each site's activation, we performed analogous experiments in benzene (all-aromatic) as well as in *tert*-butylbenzene (no benzylic C–H). Indeed, in both cases the respective signals (m/z) of the expected activation products were observed by LIFDI-MS (Figures S12 and S13; benzene: m/z = 796.094; calc = 796.094; *tert*-butylbenzene: m/z = 852.155; calc = 852.157). The presence of the respective benzene activation is further supported by the corresponding hydride signal (−16.56 ppm; Figure S7).

Taken together our experimental and computational data it is reasonable to assume that the formation of **2** proceeds via C–H activation of toluene on the electron-deficient intermedi-

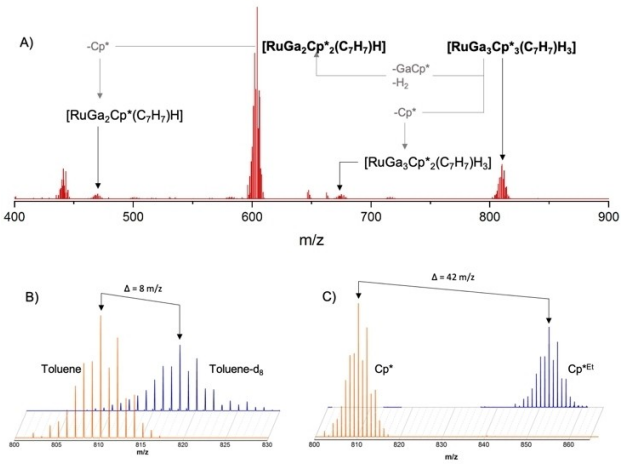


**Figure 2.** a) Size focused LIFDI-MS spectrum of **2** with the composition of the molecular ion and the main fragments given. b) LIFDI-MS patterns of **2** for the reaction in toluene and the labeling experiment using toluene-d$_8$ and c) the LIFDI-MS patterns of **2** with Cp* and Cp*$^{Et}$. The m/z difference of 8 and 42 respectively shows the incorporation of one toluene and three Cp* into the compound.

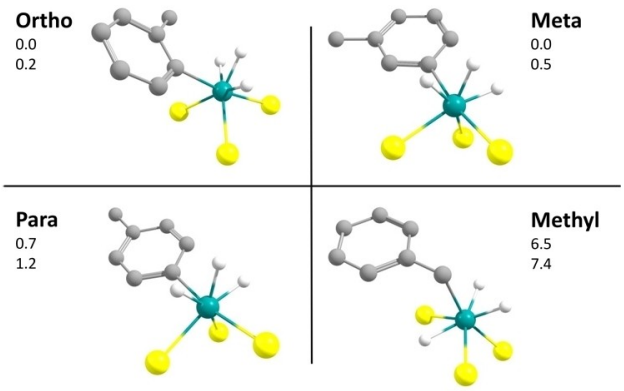


**Figure 3.** Calculated isomers of **2** with their relative total (ΔE) and free (ΔG) energy differences in kcal/mol (top: ΔE; bottom:ΔG). Cp* and hydrogen atoms of toluene omitted for clarity.

ate $[(Cp^*Ga)_3RuH_2]$.[25] To validate this hypothesis, the hydrogenolysis of ruthenium complexes with GaCp* was performed in *n*-hexane to prevent C–H or Si–H activation. This may lead to the activation of a second $H_2$ equivalent.[38] While there is no experimental evidence for a potential $[(Cp^*Ga)_3RuH_4]$, cluster growth reactions are observed by LIFDI-MS (Figure S14). This points to reactive intermediates and related competing reactions between bond activation (in aromatic solvents or silane) and cluster growth.

Starting from $[(Cp^*Ga)_3RuH_2]$, DFT calculations allow the rationalization of the observed reactivity from a thermodynamic point of view. C–H activation of toluene at $[(Cp^*Ga)_3RuH_2]$ is thermodynamically favorable according to free energy calculations ($\Delta G = -11.8$ kcal/mol). Note that replacing toluene by benzene barely changes the reaction energy ($\Delta G = -11.3$ kcal/mol). Replacing $[(Cp^*Ga)_3RuH_2]$ by its hypothetical phosphine-ligated analogue $[(PMe_3)_3RuH_2]$ cancels the exergonicity of the toluene C–H activation reaction ($\Delta G = +1.4$ kcal/mol). A similar trend and energetic difference are found for the Si–H addition of $HSiEt_3$ on the same electron-deficient species. In the case of $[(Cp^*Ga)_3RuH_2]$, $\Delta G = -43.1$ kcal/mol, whereas in the case of $[[(PMe_3)_3RuH_2]$, $\Delta G = -28.8$ kcal/mol.

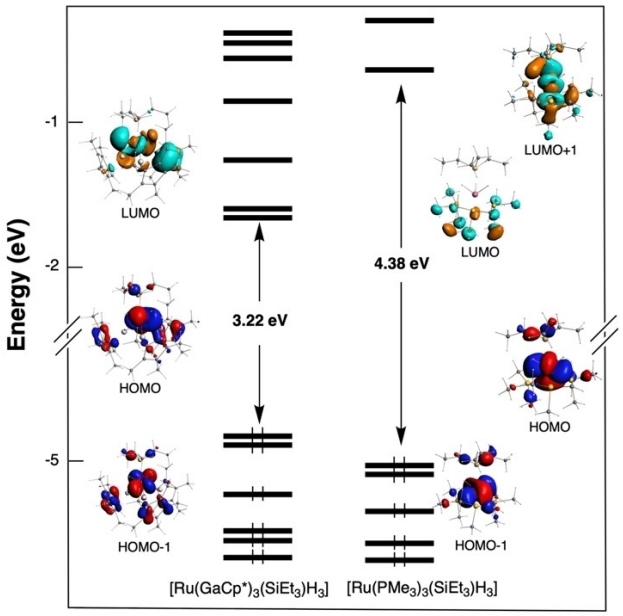


**Figure 4.** Kohn-Sham MO diagrams of **1** and $[Ru(PMe_3)_3(SiEt_3)H_3]$.

### Theoretical investigations on the Ru-Ga and Ru-P bonding

Both **1** and $[Ru(PMe_3)_3(SiEt_3)H_3]$ are hepta-coordinated Ru(IV) 18 VE complexes that can be described as made of a pseudo-octahedral $[RuL_3H_3]$ (L = GaCp*, $PMe_3$) unit to which an $SiEt_3$ ligand is added along the $C_3$ axis. The four Ru(IV) electrons are expected to occupy non-bonding 4d orbitals, i.e., those which do not point towards ligands, namely MOs of dominant xy and $x^2$-$y^2$ character (considering the z axis colinear with the Ru–Si bond). As shown by the Kohn-Sham orbital diagrams of **1** and $[Ru(PMe_3)_3(SiEt_3)H_3]$ (Figure 4), these two orbitals are the HOMO and HOMO-1 of the complexes. Despite their qualitatively related electronic structures, both complexes have some differences, as exemplified by their HOMO-LUMO gaps, that of **1** being much lower than that of its phosphine analogue. The lowest metal-ligand antibonding orbital of **1** is its LUMO, whereas it is the LUMO + 1 in the phosphine complex. Selected computed data for both complexes are gathered in Table S1. They show roughly similar bond distances around Ru in both complexes, with similar Wiberg indices, which however indicate that the Ru–Ga bonding is somewhat weaker than the Ru–P one. To gain deeper insights into the Ru–L (L = GaCp*, $PMe_3$) bonding in **1** and $[Ru(PMe_3)_3(SiEt_3)H_3]$, we performed an energy decomposition analysis (EDA) of the interaction between two frozen molecular fragments, according to the Morokuma-Ziegler procedure.[39–41] The decomposition of the total bonding energy (TBE) between the $[RuH_3(SiEt_3)]$ fragment and its $L_3$ shell is provided in Table 1. TBE is expressed as the sum of four components: the Pauli repulsion ($E_{Pauli}$), the electrostatic interaction energy ($E_{elstat}$), the orbital interaction energy ($E_{orb}$) and the component associated with the dispersion forces ($E_{disp}$). From comparing these TBE values, it is clear that the Ru–L bonding is stronger in the case where L = $PMe_3$ than for L = GaCp*. Whereas the $E_{Pauli}$ and $E_{elstat}$ components of the two compounds differ significantly, their sum, which is often approximated to the steric part of the interaction energy are about the same ($E_{Steric} = 2.37$ and 2.48 eV for L = GaCp* and $PMe_3$, respectively). Since the $E_{disp}$ contributions are also similar, the TBE main difference originates from the $E_{orb}$ components, which reflect difference in covalency. This is also consistent with the difference in the HOMO-LUMO gaps. A similar qualitative trend is found for the hypothetical unsaturated species $[Ru(GaCp^*)_3H_2]$ $[Ru(PMe_3)_3H_2]$.

Another point of view can be provided by the quantum theory of atoms in molecules (QTAIM) approach.[42–43] Selected QTAIM data associated with the Ru–Ga/P bond critical points in **1** and $[Ru(PMe_3)_3(SiEt_3)H_3]$ are collated in Table S2. In both

**Table 1.** Morokuma-Ziegler energy decomposition analysis of 1, $[Ru(GaCp^*)_3H_2]$, and their trimethylphosphine analogues. All values are in eV.

| Com-pound<br>Fragmentation | $[Ru(GaCp^*)_3(SiEt_3)H_3]$ (1)<br>$[RuH_3(SiEt_3)] + [GaCp^*]_3$ | $[Ru(PMe_3)_3(SiEt_3)H_3]$<br>$[RuH_3(SiEt_3)] + [PMe_3]_3$ | $[Ru(GaCp^*)_3H_2]$<br>$[RuH_2] + [GaCp^*]_3$ | $[Ru(PMe_3)_3H_2]$<br>$[RuH_2] + [PMe_3]_3$ |
|---|---|---|---|---|
| $E_{Pauli}$ | 11.52 | 15.19 | 11.55 | 16.94 |
| $E_{elstat}$ | −9.15 | −12.71 | −9.82 | −14.35 |
| $E_{orb}$ | −5.99 | −8.04 | −6.86 | −9.67 |
| $E_{disp}$ | −1.45 | −1.36 | −0.84 | −0.94 |
| TBE[a] | −5.08 | −6.93 | −5.97 | −8.02 |

compounds, the positive value of the Laplacian density, the negative values of the energy and potential energy densities and the larger than 1 |V|/G ratio are not contradicting the typical description of a ligand-to-metal dative bonding in both compounds.[44–46] The delocalization index is indicative of a weaker Ru–Ga covalent interaction, in agreement with the EDA analysis and Wiberg bond indices. The AIM charges indicate a more negatively polarized Ru in the case of Ru–Ga as compared to Ru–P. This points to a bond polarization of the form TM($\delta^-$)-E($\delta^+$), which could already be expected from previous reports,[19,22–23, 31] As shown in Tables 1, S1 and S2, the Ru–Ga vs. Ru–P bonding features are maintained on the hypothetical 16 VE intermediates [$RuL_3H_2$] (L = GaCp*, $PMe_3$).

## Conclusion

Ru/Ga complexes have been investigated with respect to their behavior in C–H and Si–H bond activation reactions. [Ru-$(GaCp^*)_3H_2$] has been proposed as the crucial intermediate in the bond activation reactions, DFT calculations confirming the increased reactivity with respect to the phosphine analogue [$Ru(PMe_3)_3H_2$].

[$Ru(GaCp^*)_3H_2$] has also been described in earlier studies as a reactive intermediate on the way to Ru/Ga clusters. Thus, reductive elimination of Cp*H leads to a ligand stabilized Ru/Ga cluster with a linear Ru–Ga-Ru backbone.[25] This underlines the crucial role of transient and/or intermediate species in cluster growth reactions. The "proto" cluster species [$Ru(GaCp^*)_3H_2$] obviously can act as a reactive building block for larger clusters, whereby substrate (e.g. $H_2$) or solvent molecules actively intervene in the reaction process by stabilizing the intermediate. Controlling the resulting complexity often remains a challenge. One possible approach to control cluster growth, however, which has been recently successfully employed in the synthesis of Ni/Al and Ni/Ga clusters is the use of alkynes as additives.[47] A propagation of this idea with the aim of investigating larger Ru/Ga clusters is part of an ongoing project and will be presented in future work.

## Experimental Section

**General remarks**: All manipulations were carried out using standard Schlenk techniques under inert atmospheres. Solvents were dried using a MBraun Solvent Purification System. The final $H_2O$ content of all solvents was measured via Karl Fischer titration and was below 5 ppm. Starting materials [$Ru(COD)(MeAllyl)_2$], [Ru-(COD)(COT)] and GaCp* were synthesized according to literature procedures. Elemental analysis was conducted at the microanalytical laboratory at the Technical University Munich. NMR spectra were recorded on a Bruker AVIII 400 US spectrometer ($^1$H, 400 MHz; $^{13}$C, 101 MHz) in $C_6D_6$. Chemical shifts (in δ) are described in ppm relative to tetramethylsilane (TMS) and referenced to the solvent resonances as internal standards. The signal multiplicity is given as following: s = singlet, d = doublet, t = triplet or q = quartet.

**LIFDI-MS**: Liquid Injection Field Desorption Ionization Mass Spectrometry (LIFDI-MS) was measured directly from an inert atmosphere glovebox with a Thermo Fisher Scientific Exactive Plus Orbitrap (mass accuracy 3 ppm; external calibration) equipped with an ion source from Linden CMS.[48]

**Crystallography**: For compound **1** X-ray diffraction intensities were collected on a Bruker D8-Venture diffractometer equipped with a CMOS detector (Bruker Photon- 100), an IMS microfocus with Mo $K_\alpha$ radiation (λ = 0.71073 Å) and a Helios optic. Suitable crystals were coated in perfluoropolyether and mounted in the cooled nitrogen stream (100 K) of the diffractometer on a kapton microsampler. Diffraction data were processed with APEX III and the implemented SAINT and SADABS programs. Structures were solved using SHELXT and refined with SHELXL-2017 in conjunction with SHELXLE. Further crystallographic details are provided in the Supporting Information.

Deposition Number(s) 2158227 (**1**) contain(s) the supplementary crystallographic data for this paper. These data are provided free of charge by the joint Cambridge Crystallographic Data Centre and Fachinformationszentrum Karlsruhe Access Structures service.

**Computational details**: Density Functional Theory (DFT) calculations were carried out with the use of the ADF2020 code[49,50] with the addition of Grimmes's D3 empirical corrections[51] to take into account dispersion effects. The triple-zeta with two polarization functions (TZ2P) basis set was used, together with the BP86[52,53] exchange-correlation functional. All the optimized structures were confirmed as true minima on their potential energy surface by analytical vibration frequency calculations. Wiberg bond indices were computed with the NBO 6.0 program[54] implemented in the ADF2020 package. The QTAIM analysis[42–43] was performed as implemented in the ADF2019 suite.[55–56] The $^1$H NMR chemical shifts were computed on the BP86/TZ2P-optimized structures, according to the GIAO method,[57] with the B3LYP functional[58] and taking into account solvent (benzene) effect via the COSMO model.[59,60]

## Synthetic protocols

[$Ru(GaCp^*)_3(SiEt_3)(H)_3$] (**1**): A solution of 450 mg (1.0 equiv., 1.410 mmol) [$Ru(COD)(MeAllyl)_2$] and 867 mg (3.0 equiv., 4.230 mmol) GaCp* in 6 mL $HSiEt_3$ is freeze-pump-thawed-degassed and pressurized with 3 bar $H_2$ in a 150 mL Fisher-Porter bottle. The reaction solution turns from yellow to dark orange over 6 h at 60 °C. Residual $HSiEt_3$ is removed in vacuo and 830 mg (71 %, 0.995 mmol) of **1** are obtained by recrystallization from *n*-hexane. $^1$H NMR ($C_6D_6$, 400 MHz): δ [ppm] = 1.88 (s, 45 H, GaCp*), 1.26 (t, 9H, $SiCH_2$-$CH_3$), 0.92 (q, 6H, Si-$H_2$C), −13.31 (s, 3H, Ru–H). $^{13}$C NMR ($C_6D_6$, 101 MHz): δ [ppm] = 113.5 (s, $C_5(CH_3)_5$), 20.2 (s, Si-$CH_2$), 10.5 (s, $SiCH_2$-$CH_3$) 10.0 (s, $C_5(CH_3)_5$). ATR-IR [$cm^{-1}$]: 1898, 1771 (Ru–H). Raman [$cm^{-1}$]: 1913 (Ru–H). UV-Vis (cyclohexane) $\lambda_{max}$ = 226 nm, 281 nm, 344 nm. LIFDI-MS m/z = 832.1313 $[M\text{-}2H]^+$. (calc = 832.1339). Elemental analysis calc. for $RuGa_3C_{36}H_{63}Si$: C, 51.83; H, 7.61; Ga, 25.07; Ru, 12.12; Si, 3.37. Found: C, 51.74; H, 7.77; Ga, 24.3; Ru, 12.0; Si, 3.79.

[$Ru(GaCp)_3(C_7H_7)H_3$] (**2**): 50.0 mg [$Ru(cod)(MeAllyl)_2$] (1.0 equiv., 0.157 mmol) and 65.0 mg GaCp* (2.0, 0.313 mmol) are inserted into a 150 mL Fisher-Porter Bottle, dissolved in 14 mL toluene. The solution is freeze-pump-thawed-degassed and pressurized with 3 bar $H_2$. The reaction mixture is stirred at 60 °C for 48 h and then canula filtrated. LIFDI-MS m/z = 810.1088 $[M]^+$ (calc = 810.1100), m/z = 604.0508 $[M\text{-}GaCp^*_2H]^+$ (calc = 604.0514).

## Acknowledgements

This work was funded by the German Research Foundation (DFG) within a Reinhard Koselleck Project (FI-502/44-1), the TUM Graduate School and the GENCI French national computer resource center (grant A0030807367). H.L. thanks the China Scholarship Council for a Ph.D. grant. The authors thank Dardan Ukaj for measuring the Raman spectrum of **1**. Open Access funding enabled and organized by Projekt DEAL.

## Conflict of Interest

The authors declare no conflict of interest.

## Data Availability Statement

The data that support the findings of this study are available from the corresponding author upon reasonable request.

**Keywords:** bond activation · cluster intermediates · density functional calculations · intermetallic compounds · mass spectrometry

[1] R. C. Cammarota, M. V. Vollmer, J. Xie, J. Ye, J. C. Linehan, S. A. Burgess, A. M. Appel, L. Gagliardi, C. C. Lu, *J. Am. Chem. Soc.* **2017**, *139*, 14244–14250.
[2] J. Fajardo, J. C. Peters, *J. Am. Chem. Soc.* **2017**, *139*, 16105–16108.
[3] I. Fujii, K. Semba, Q.-Z. Li, S. Sakaki, Y. Nakao, *J. Am. Chem. Soc.* **2020**, *142*, 11647–11652.
[4] H. Kameo, J. Yamamoto, A. Asada, H. Nakazawa, H. Matsuzaka, D. Bourissou, *Angew. Chem. Int. Ed.* **2019**, *131*, 18959–18963.
[5] R. Seki, N. Hara, T. Saito, Y. Nakao, *J. Am. Chem. Soc.* **2021**, *143*, 6388–6394.
[6] W.-C. Shih, O. V. Ozerov, *J. Am. Chem. Soc.* **2017**, *139*, 17297–17300.
[7] J. Takaya, N. Iwasawa, *J. Am. Chem. Soc.* **2017**, *139*, 6074–6077.
[8] M. V. Vollmer, J. Ye, J. C. Linehan, B. J. Graziano, A. Preston, E. S. Wiedner, C. C. Lu, *ACS Catal.* **2020**, *10*, 2459–2470.
[9] R. Yamada, N. Iwasawa, J. Takaya, *Angew. Chem. Int. Ed.* **2019**, *58*, 17251–17254; *Angew. Chem.* **2019**, *131*, 17411–17414.
[10] M. Armbrüster, K. Kovnir, M. Friedrich, D. Teschner, G. Wowsnick, M. Hahne, P. Gille, L. Szentmiklósi, M. Feuerbacher, M. Heggen, F. Girgsdies, D. Rosenthal, R. Schlögl, Y. Grin, *Nat. Mater.* **2012**, *11*, 690–693.
[11] J. Prinz, C. A. Pignedoli, Q. S. Stöckl, M. Armbrüster, H. Brune, O. Gröning, R. Widmer, D. Passerone, *J. Am. Chem. Soc.* **2014**, *136*, 11792–11798.
[12] F. Studt, F. Abild-Pedersen, T. Bligaard, Z. Sørensen Rasmus, H. Christensen Claus, K. Nørskov Jens, *Science* **2008**, *320*, 1320–1322.
[13] M. Armbrüster, *Sci. Technol. Adv. Mater.* **2020**, *21*, 303–322.
[14] J. Campos, *Nat. Chem. Rev.* **2020**, *4*, 696–702.
[15] S. Furukawa, T. Komatsu, *ACS Catal.* **2017**, *7*, 735–765.
[16] K. Mayer, J. Weßing, T. F. Fässler, R. A. Fischer, *Angew. Chem. Int. Ed.* **2018**, *57*, 14372–14393; *Angew. Chem.* **2018**, *130*, 14570–14593.
[17] T. Steinke, C. Gemel, M. Cokoja, M. Winter, R. A. Fischer, *Angew. Chem. Int. Ed.* **2004**, *116*, 2349–2352.
[18] T. Cadenbach, C. Gemel, R. Schmid, R. A. Fischer, *J. Am. Chem. Soc.* **2005**, *127*, 17068–17078.
[19] R. H. Crabtree, D. G. Hamilton, *J. Am. Chem. Soc.* **1986**, *108*, 3124–3125.
[20] R. O. Harris, N. K. Hota, L. Sadavoy, J. M. C. Yuen, *J. Organomet. Chem.* **1973**, *54*, 259–264.
[21] S. Wesselbaum, T. vom Stein, J. Klankermayer, W. Leitner, *Angew. Chem. Int. Ed.* **2012**, *51*, 7499–7502; *Angew. Chem.* **2012**, *124*, 7617–7620.
[22] Z. Ruan, S.-K. Zhang, C. Zhu, P. N. Ruth, D. Stalke, L. Ackermann, *Angew. Chem. Int. Ed.* **2017**, *56*, 2045–2049; *Angew. Chem.* **2017**, *129*, 2077–2081.
[23] E. L. Dias, S. T. Nguyen, R. H. Grubbs, *J. Am. Chem. Soc.* **1997**, *119*, 3887–3897.
[24] V. K. Dioumaev, L. J. Procopio, P. J. Carroll, D. H. Berry, *J. Am. Chem. Soc.* **2003**, *125*, 8043–8058.
[25] T. Cadenbach, C. Gemel, R. Schmid, M. Halbherr, K. Yusenko, M. Cokoja, R. A. Fischer, *Angew. Chem. Int. Ed.* **2009**, *48*, 3872–3876; *Angew. Chem.* **2009**, *121*, 3930–3934.
[26] R. A. Fischer, J. Weiß, *Angew. Chem. Int. Ed.* **1999**, *38*, 2830–2850; *Angew. Chem.* **1999**, *111*, 3002–3022.
[27] J. Hornung, J. Weßing, P. Jerabek, C. Gemel, A. Pöthig, G. Frenking, R. A. Fischer, *Inorg. Chem.* **2018**, *57*, 12657–12664.
[28] M. Muhr, J. Hornung, J. Weßing, C. Jandl, C. Gemel, R. A. Fischer, *Inorg. Chem.* **2020**, *59*, 5086–5093.
[29] T. Steinke, C. Gemel, M. Winter, R. A. Fischer, *Chem. Eur. J.* **2005**, *11*, 1636–1646.
[30] J. Uddin, C. Boehme, G. Frenking, *Organometallics* **2000**, *19*, 571–582.
[31] J. Uddin, G. Frenking, *J. Am. Chem. Soc.* **2001**, *123*, 1683–1693.
[32] W. Uhl, M. Benter, S. Melle, W. Saak, G. Frenking, J. Uddin, *Organometallics* **1999**, *18*, 3778–3780.
[33] B. Buchin, C. Gemel, A. Kempter, T. Cadenbach, R. A. Fischer, *Inorg. Chim. Acta* **2006**, *359*, 4833–4839.
[34] T. Cadenbach, T. Bollermann, C. Gemel, R. A. Fischer, *Dalton Trans.* **2009**, 322–329.
[35] T. Cadenbach, C. Gemel, T. Bollermann, I. Fernandez, G. Frenking, R. A. Fischer, *Chem. Eur. J.* **2008**, *14*, 10789–10796.
[36] B. Chatterjee, C. Gunanathan, *Chem. Commun.* **2014**, *50*, 888–890.
[37] T. Komuro, H. Tobita, *Chem. Commun.* **2010**, *46*, 1136–1137.
[38] B. Chaudret, R. Poilblanc, *Organometallics* **1985**, *4*, 1722–1726.
[39] F. M. Bickelhaupt, E. J. Baerends, in *Rev. Comput. Chem, Vol. 15* (Eds.: K. B. Lipkowitz, D. B. Boyd), Wiley, New-York, **2000**, pp. 1–86.
[40] K. Morokuma, *J. Chem. Phys.* **1971**, *55*, 1236–1244.
[41] T. Ziegler, R. Arvi, *Inorg. Chem.* **1979**, *18*, 1558–1565.
[42] R. F. W. Bader, *Atoms in Molecules - A Quantum Theory*, Oxford University Press, **1990**.
[43] P. L. A. Popelier, in *The Chemical Bond, Vol. 1*, Wiley-VCH, **2014**, pp. 271–308.
[44] A. A. Adeniyi, P. A. Ajibade, *J. Biomol. Struct. Dyn.* **2014**, *32*, 1351–1365.
[45] R. Gericke, J. Wagler, *Inorg. Chem.* **2020**, *59*, 6359–6375.
[46] C. Lepetit, P. Fau, K. Fajerwerg, M. L. Kahn, B. Silvi, *Coord. Chem. Rev.* **2017**, *345*, 150–181.
[47] P. Heiß, J. Hornung, C. Gemel, R. A. Fischer, *Chem. Commun.* **2022**, 58, 4332–4335.
[48] M. Muhr, P. Heiß, M. Schütz, R. Bühler, C. Gemel, M. H. Linden, H. B. Linden, R. A. Fischer, *Dalton Trans.* **2021**, *50*, 9031–9036.
[49] G. te Velde, F. M. Bickelhaupt, E. J. Baerends, C. Fonseca Guerra, S. J. A. van Gisbergen, J. G. Snijders, T. Ziegler, *J. Comput. Chem.* **2001**, *22*, 931–967.
[50] E. J. Baerends, T. Ziegler, A. J. Atkins, J. Autschbach, D. Bashford, O. Baseggio, A. Bérces, F. M. Bickelhaupt, C. Bo, P. M. Boerritger, L. Cavallo, C. Daul, D. P. Chong, D. V. Chulhai, L. Deng, R. M. Dickson, J. M. Dieterich, D. E. Ellis, M. van Faassen, A. Ghysels, A. Giammona, S. J. A. van Gisbergen, A. Goez, A. W. Götz, S. Gusarov, F. E. Harris, P. van den Hoek, Z. Hu, C. R. Jacob, H. Jacobsen, et al., SCM, **2020**.
[51] S. Grimme, *J. Comput. Chem.* **2006**, *27*, 1787–1799.
[52] A. D. Becke, *Phys. Rev. A* **1988**, *38*, 3098–3100.
[53] J. P. Perdew, *Phys. Rev. B* **1986**, *33*, 8822–8824.
[54] E. D. Glendening, C. R. Landis, F. Weinhold, *J. Comput. Chem.* **2013**, *34*, 1429–1437.
[55] J. I. Rodríguez, *J. Comput. Chem.* **2012**, *34*, 681–686.
[56] J. I. Rodríguez, R. F. W. Bader, P. W. Ayers, C. Michel, A. W. Götz, C. Bo, *Chem. Phys. Lett.* **2009**, *472*, 149–152.
[57] G. Schreckenbach, T. Ziegler, *J. Phys. Chem.* **1995**, *99*, 606–611.
[58] P. J. Stephens, F. J. Devlin, C. F. Chabalowski, M. J. Frisch, *J. Phys. Chem.* **1994**, *98*, 11623–11627.
[59] A. Klamt, G. Schüürmann, *J. Chem. Soc. Perkin Trans. 2* **1993**, 799–805.
[60] A. Klamt, *J. Phys. Chem.* **1995**, *99*, 2224–2235.

Manuscript received: March 21, 2022
Accepted manuscript online: June 24, 2022
Version of record online: ■■, ■■■

# RESEARCH ARTICLE

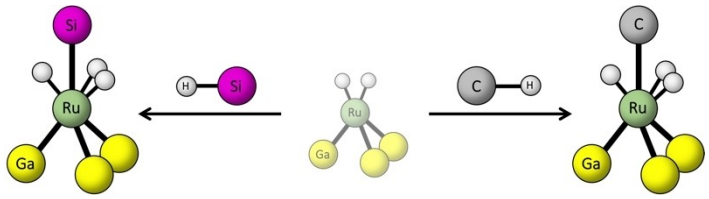


**Ru/Ga compounds** activate Si–H and C–H bonds. Triethylsilane and toluene are activated by the intermediate [Ru-$(GaCp^*)_3H_2$] and form the respective seven-fold coordinated Ru/Ga species. The bonding situation of the intermediate, the products, and their respective phosphine analogues are analyzed on the DFT level of theory, and the Ru–Ga and Ru–P bond are contrasted.

*M. Muhr, R. Bühler, H. Liang, J. Gilch, Dr. C. Jandl, Dr. S. Kahlal, Prof. Dr. J.-Y. Saillard*, Dr. C. Gemel, Prof. Dr. R. A. Fischer**